THE JOURNAL OF PHYSICAL CHEMISTRY A

pubs.acs.org/JPCA Article

Deprotonation of Guanine Radical Cation $G^{\bullet+}$ Mediated by the Protonated Water Cluster

Xianwang Zhang, Jialong Jie,* Di Song,* and Hongmei Su

Cite This: J. Phys. Chem. A 2020, 124, 6076−6083 Read Online

ACCESS | Metrics & More | Article Recommendations | Supporting Information

ABSTRACT: Proton transfer is regarded as a fundamental process in chemical reactions of DNA molecules and continues to be an active research theme due to the connection with charge transport and oxidation damage of DNA. For the guanine radical cation ($G^{\bullet+}$) derived from one-electron oxidation, experiments suggest a facile proton transfer within the $G^{\bullet+}$:C base pair, and a rapid deprotonation from N1 in free base or single-strand DNA. To address the deprotonation mechanism, we perform a thorough investigation on deprotonation of $G^{\bullet+}$ in free G base by combining density functional theory (DFT) and laser flash photolysis spectroscopy. Experimentally, kinetics of deprotonation is monitored at temperatures varying from 280 to 298 K, from which the activation energy of 15.1 ± 1.5 kJ/mol is determined for the first time. Theoretically, four solvation models incorporating explicit waters and the polarized continuum model (PCM), i.e., $3H_2O$-PCM, $4H_2O$-PCM, $5H_2O$-PCM, and $7H_2O$-PCM models are used to calculate deprotonation potential energy profile, and the barriers of 5.5, 13.4, 14.4, and 13.7 kJ/mol are obtained, respectively. It is shown that at least four explicit waters are required for properly simulating the deprotonation reaction, where the participation of protonated water cluster plays key roles in facilitating the proton release from $G^{\bullet+}$.

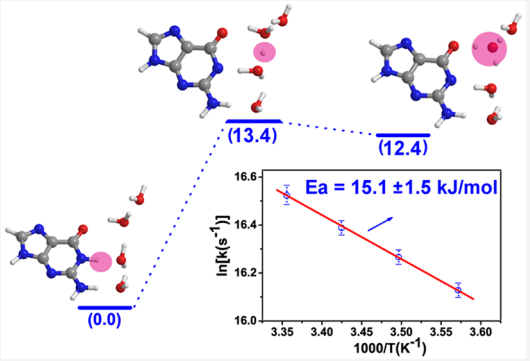

INTRODUCTION

Proton transfer through hydrogen bonds attracts continuous interests and massive research efforts, because of the significance in most essential chemical and biological processes.[1−10] Many theoretical and experimental investigations show that molecular mechanism behind proton transfer probably involves protonated water clusters.[1−7] Two important structures of protonated water clusters, $H^+(H_2O)_4$ with a central hydronium core (H_3O^+) bound to three waters[1] and $H^+(H_2O)_2$ possessing a proton fluctuating between two waters,[2] are proposed to explain anomalously high proton mobility of liquid water.[3] Unlike other ions, the transport of protons in aqueous solution does not require the net diffusion of ionic species but instead is driven by a periodic series of isomerizations between $H^+(H_2O)_4$ and $H^+(H_2O)_2$, where the charge is transferred along the hydrogen bond.[3,6,10] Even for proton transfer across biomembranes such as bacteriorhodopsin, which affects biological functions of protein assemblies, the suggested mechanism also emphasizes the participations of protonated water clusters based on time-resolved Fourier transform infrared spectroscopy (trFTIR) and *in situ* $H_2{}^{18}O/H_2{}^{16}O$ exchange FTIR measurements.[11]

Interestingly, proton transfer is also a universal phenomenon in chemical reactions of DNA molecules, the mechanism of which continues to be an active research theme because of the connection with charge transport and oxidation damage of DNA. Following one-electron oxidation of DNA, for example, the instantaneously generated guanine radical cation ($G^{\bullet+}$) can undergo rapid proton transfer, competing with hole transfer along DNA or leading to oxazolone via further reaction of its product, guanine radical $G(-H)^{\bullet}$.[12−24] As shown in Scheme 1, $G^{\bullet+}$ has two sites, N1−H (pK_a = 3.9) and N2−H (pK_a = 4.7), to lose a proton. According to the pK_a values, the N1−H site is suggested to be favored over the N2−H site. Pulse radiolysis[12,17] and ESR[18] experiments showed that only $G(N1-H)^{\bullet}$ were observed in the aqueous phase after proton transfer at pH = 7.0. Density functional theory (DFT) calculations including seven water molecules as the hydration shell also provided a theoretical support that $G(N1-H)^{\bullet}$ is more stable than $G(N2-H)^{\bullet}$ by 13.6 kJ/mol.[18] Therefore, the proton transfer of $G^{\bullet+}$ in free nucleobase is thought to occur at the N1−H site.

It is noticeable that in different DNA structures, mechanisms of proton transfer of $G^{\bullet+}$ are different. In the DNA duplex, a facile proton transfer from N1 of $G^{\bullet+}$ to N3 of hydrogen-bonded cytosine (C) within the G:C base pair was proposed (Scheme 1),[12,16,21,22,25,26] since the pK_a (4.3) of N3-protonated cytosine is higher than that of $G^{\bullet+}$. Both transient

Received: April 27, 2020
Revised: June 24, 2020
Published: June 25, 2020

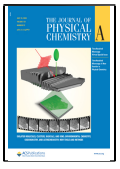

Downloaded via BEIJING NORMAL UNIV on September 25, 2020 at 08:35:17 (UTC).
See https://pubs.acs.org/sharingguidelines for options on how to legitimately share published articles.

ACS Publications © 2020 American Chemical Society

https://dx.doi.org/10.1021/acs.jpca.0c03748
J. Phys. Chem. A 2020, 124, 6076−6083

Scheme 1. (a) Proton Transfer (PT) Reaction in a One-Electron Oxidized G:C Base Pair and (b) Deprotonation from N1 and N2 Site of Guanine Radical Cation, Respectively

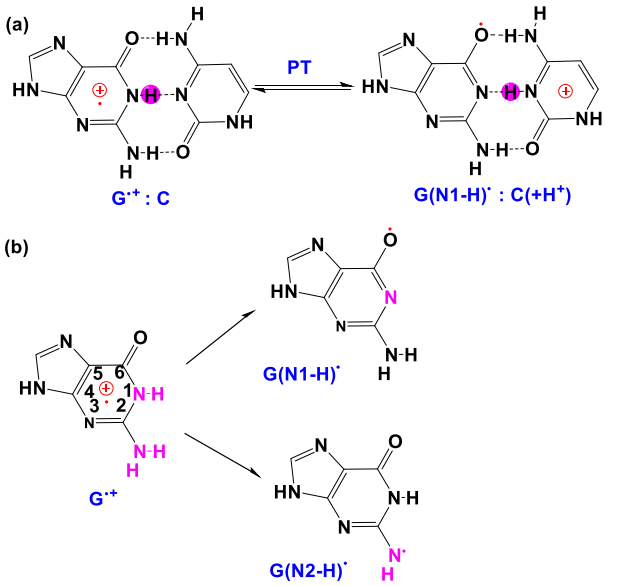

absorption spectra and kinetics measurements further confirmed this intrabase proton transfer route.[17,21,27] An earlier DFT study on isolated $G^{\bullet+}$:C base pair in the gas phase predicted that the interbase proton transfer is unfavorable as the product G(N1−H)•:C(+H)$^+$ is 5.9 kJ/mol less stable than the reactant $G^{\bullet+}$:C, conflicting with experimental results.[16] Upon incorporation of 11 water molecules around the $G^{\bullet+}$:C, the B3LYP/6-31+G** calculations showed that the G(N1−H)•:C(+H)$^+$ becomes more stable than the $G^{\bullet+}$:C by 5.0 kJ/mol, settling this controversy.[22] It follows that hydration effect plays an important role in reaction energetics, although the intrabase proton transfer within the $G^{\bullet+}$:C base pair takes place in a hydrophobic environment.

In free base, single-strand DNA and triplex DNA, $G^{\bullet+}$ transfers the N1−H proton to surrounding waters,[12−14,17,18,20,23,28] namely, deprotonation. Since the N1−H site of $G^{\bullet+}$ is not hydrogen-bonded with the C base anymore and then has access to water, it is intriguing to investigate the role of water cluster or protonated water cluster in the process of proton transfer of $G^{\bullet+}$. However, the deprotonation mechanism of $G^{\bullet+}$ has not been addressed properly. In a theoretical investigation on mechanisms of peroxynitrite oxidation of guanine,[29] B3LYP calculations involving one water molecule presented a free energy profile of $G^{\bullet+}$ deprotonation, in which the transition state was located, with an energy of 65.8 kJ/mol above the reactants. Unfortunately, there is hitherto no reported experimental activation energy to be compared with. Assuming the energy barrier is 65.8 kJ/mol, deprotonation should take place on the time scale of milliseconds, which is obviously in disagreement with the nanoseconds (1.8×10^7 s^{-1}) rates observed in experiments.[17]

In this context, we performed a joint theoretical and experimental investigation on deprotonation of $G^{\bullet+}$ derived from one-electron oxidation of free G base. With the transient absorption spectroscopy, the dependence of formation kinetics of G(N1−H)• on temperatures was measured, from which the activation energy of deprotonation was determined. To provide further mechanistic insights, potential energy profiles of deprotonation were calculated under solvation models incorporating explicit waters and the polarized continuum model (PCM), which provide energy barriers matching the experimental value and thus suggest a deprotonation process assisted by protonated water cluster. The deprotonation mechanism of $G^{\bullet+}$ in free base after one-electron oxidation is clarified, revealing the crucial role of protonated water cluster. These results enrich understandings for proton transfer of DNA systems, which are closely associated with hole transfer along DNA and oxidative damage of DNA.

MATERIALS AND METHODS

Materials. 2′-Deoxyguanosine (G, Alfa Aesar), sodium persulfate ($Na_2S_2O_8$, Sigma-Aldrich), and sodium phosphate buffer (50 mM, Beijing Solarbio Science & Technology) were used as purchased. Ultrapure water obtained by Millipore filtration was used as solvent. The sample of G and $Na_2S_2O_8$ (ca. 0.215 g) was dissolved in 3 mL of sodium phosphate buffer (50 mM, pH 7.0) in H_2O.

Laser Flash Photolysis. Nanosecond time-resolved transient absorption spectra were measured using a flash photolysis setup Edinburgh LP920 spectrometer (Edinburgh Instruments Ltd.) combined with a Nd:YAG laser (Spectra-Physics Lab 170, Newport Corp.).[30,31] Each measurement was performed in a 1 cm path length quartz cuvette that was put in the Oxford Instruments OptistatDN Cryostat and cooled to a certain temperature. The sample was excited by using a 355 nm laser pulse (1 Hz; 20 mJ/pulse; full width at half-maximum, ≈ 7 ns). The analyzing light was from a 450 W pulsed xenon lamp. A monochromator equipped with a photomultiplier for collecting the spectral range from 300 to 700 nm was used to analyze transient absorption spectra. The signals from the photomultiplier were displayed and recorded as a function of time on a 100 MHz (1.25 Gs/s sampling rate) oscilloscope (TDS 3012C, Tektronix), and the data were transferred to a PC. Data were analyzed with online software of the LP920 spectrophotometer and instrument response function of Gaussian type was considered. The fitting quality was judged by weighted residuals and reduced χ^2 value. Note that each kinetic measurement was performed with new sample.

Computational Methods. The geometries were fully optimized using the M06-2X density functional in connection with the 6-31++G** basis set and the polarized continuum model. M06-2X developed by Truhlar and Zhao is a hybrid meta functional having 54% Hartree−Fock exchange contribution.[32,33] Due to the large exchange−correlation, this functional is a better choice than other functions, for example, B3LYP, which is severely influenced by the self-interaction error.[34] The M06-2X functional has been shown to well describe noncovalent interactions; thus, it is very suitable for studying a number of chemical problems, including radicals and hydrated molecule ions.[32,35−37] For example, Johnson et al. used the M06-2X functional with the 6-31++G** basis set to obtain vibration spectra of $[Py^{\bullet}(H_2O)_{n=3-5}]^-$ radical anions and the potential energy curve for proton transfer in $[Py^{\bullet}(H_2O)_3]^-$, revealing the important role of proton-assisted charge accommodation in electron capture by a heterocyclic electron scavenger.[37] To ensure the suitability of the M06-2X functional to treat our study system, other common density functionals, BP86, PBE, and B3LYP, at the same level with the

https://dx.doi.org/10.1021/acs.jpca.0c03748
J. Phys. Chem. A 2020, 124, 6076−6083

6-31++G** basis set were employed in the parallel calculations. As shown in Table S1, the calculated energy barrier of M06-2X agrees well with our experimental result, while those of other functionals deviate to varying degrees. Additionally, to consider long-range electron correlation, the M06-2X functional was also added to empirical terms that model dispersion interactions. It is shown that energy barriers calculated using the M06-2X-D3 functional in Table S1 are similar to the results of the M06-2X functional. The M06-2X functional in connection with the 6-31++G** basis set can provide a useful and affordable method and was thus chosen in this work.

The harmonic frequency analysis was performed to identify the stationary point as either local minima (reactant and products) or first-order saddle points (transition states) and to extract zero-point vibrational energy (ZPE) corrections. Connections of the transition states between two local minima were confirmed by intrinsic reaction coordinate (IRC) calculations at the same level. Partial atomic charges using the natural bond orbital (NBO) scheme and spin densities were evaluated at the same level. All the calculations were carried out using the Gaussian 09 program package.[38]

RESULTS AND DISCUSSION

In this work, laser flash photolysis experiments were first performed to obtain the activation energy of $G^{\bullet+}$ deprotonation. It is well-known that the $SO_4^{\bullet-}$ oxidizes G to $G^{\bullet+}$ and $G^{\bullet+}$ deprotonates to $G(N1-H)^{\bullet}$ by rapid loss of the imino proton at pH 7.0 (reactions 2 and 3).[23,39,40] In our experiments, the oxidizing radicals $SO_4^{\bullet-}$ are generated within the ~14 ns laser pulse duration through the rapid photodissociation of $S_2O_8^{2-}$ by 355 nm laser irradiation (reaction 1),[23,24,31,39,41] which ensures no interference with the detection of the oxidation reaction with G and subsequent deprotonation. According to previous pulse radiolysis studies,[17] when the concentration of G is above 3 mM, the deprotonation of $G^{\bullet+}$ to $G(N1-H)^{\bullet}$, rather than the bimolecular reaction of $SO_4^{\bullet-}$ oxidizing G, is the rate-determining step of the $G(N1-H)^{\bullet}$ formation (reactions 2 and 3). Hence, a high concentration of G (6 mM) was used in this experiment, to monitor the deprotonation kinetics of $G^{\bullet+}$ to $G(N1-H)^{\bullet}$ through the time-resolved spectra.

$$S_2O_8^{2-} \xrightarrow{h\nu} 2SO_4^{\bullet-} \quad (1)$$

$$SO_4^{\bullet-} + G \rightarrow SO_4^{2-} + G^{\bullet+} \quad (2)$$

$$G^{\bullet+} \rightarrow G(-H)^{\bullet} + H^{+} \quad (3)$$

Figure 1a shows that transient absorption spectra at different time delays upon the 355 nm photolysis of G and $Na_2S_2O_8$ mixture. The 60 ns spectrum is featured with two resolved bands at 380 and 510 nm as well as a flat absorption above 600 nm, which are essentially similar to those reported before and can thus be identified as the mixture of $G^{\bullet+}$ and $G(N1-H)^{\bullet}$.[17,21,23,24] As the reaction proceeds with time, $G(N1-H)^{\bullet}$ continues to be generated and its proportion in the mixture increases accordingly. According to previous experimental spectra[17,42,43] as well as calculated absorption spectra of $G^{\bullet+}$ and $G(N1-H)^{\bullet}$,[44,45] $G(N1-H)^{\bullet}$ exhibits a stronger absorption around 380 nm and above 500 nm compared with results for $G^{\bullet+}$. Therefore, the absorptions around 380 nm and above 500 nm pronouncedly increase in the 120 and 200 ns spectra,

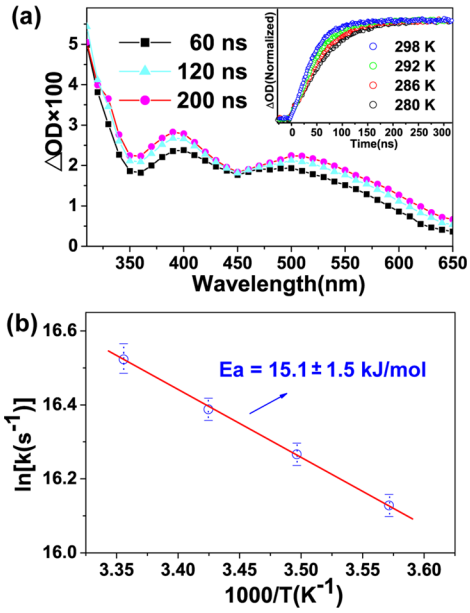

Figure 1. (a) Transient UV−vis spectra for solution of G (6 mM) + $Na_2S_2O_8$ at 298 K upon 355 nm laser flash photolysis. Insert: kinetic curves monitored at 625 nm at temperatures varying from 280 to 298 K. (b) Arrhenius plots for the temperature dependence (298, 292, 286, 280 K) of the rate constants measured respectively from the absorbance changes at 625 nm, with the activation energy indicated. Solid red line is the fit.

which mainly correspond to $G(N1-H)^{\bullet}$. To obtain the rate constant of deprotonation, the absorption change of 625 nm where $G(N1-H)^{\bullet}$ mainly absorbs was measured in H_2O at 298 K (the inset of Figure 1a). Through a monoexponential fitting, the deprotonation rate constant can thus be determined as 1.5×10^7 s^{-1}, which is in accord with nanosecond pulse radiolysis result (1.8×10^7 s^{-1}) by Kobayashi and coworkers.[17]

The deprotonation rate constant as a function of temperature in the range 280−298 K was measured to obtain the activation energy of $G^{\bullet+}$ deprotonation. Note that here at a higher temperature above room temperature 298 K, the deprotonation rate constant is too fast to be measured within the nanosecond time resolution, while for a much lower temperature condition, antifreeze is required in the experiment to avoid the solution becoming untransparent, which in turn invokes additional reaction processes. As shown in Figure 1b, the deprotonation rate constants decrease with the temperature, and the rate constants exhibit an Arrhenius behavior. The Arrhenius plot yields an energy barrier of 15.1 ± 1.5 kJ/mol, corresponding to the activation energy of $G^{\bullet+}$ deprotonation. To the best of our knowledge, the experimental activation energy of N1-dprotonation of $G^{\bullet+}$ is for the first time reported.

To shed light on mechanistic aspects, a computational investigation of deprotonation mechanism of $G^{\bullet+}$ by loss of a proton from the N1−H site to the surrounding waters was performed at the M06-2X/6-31++G** level. In the previous study, rate constants of $G^{\bullet+}$ deprotonation in H_2O and D_2O were measured to be 1.7×10^7 s^{-1} (k_H) and 1.0×10^7 s^{-1} (k_D), respectively, showing a k_H/k_D of 1.7.[21] Obviously, this is a quite small kinetic isotope effect, thereby one can deduce that deprotonation of $G^{\bullet+}$ should not incorporate a tunneling effect.[46−52]

https://dx.doi.org/10.1021/acs.jpca.0c03748
J. Phys. Chem. A 2020, 124, 6076−6083

Since hydration is crucial for intrabase proton transfer within the $G^{\bullet+}$:C base pair, the solvation effect should also be considered carefully in the calculations here. To properly mimic the surrounding environment of $G^{\bullet+}$ in the free base, four solvation models are proposed by using the PCM and explicit waters in a hydration shell, which usually reflects the electrostatic interaction and hydrogen-bonding interaction between solute and solvent, respectively. The four models are denoted as $3H_2O$-PCM, $4H_2O$-PCM, $5H_2O$-PCM, and $7H_2O$-PCM.

Figure 2a plots arrangement of explicit water molecules in the $4H_2O$-PCM model. Three waters (W1, W2, and W3) are placed in the first hydration shell, near N1, N2, and O6 of $G^{\bullet+}$ in the hydrogen-bonding conformation. The fourth one (W4) merely interacts with W3 via a relative weaker hydrogen bond, which represents the effect of the second hydration shell. According to our calculations, the role of W4 should be to help the proton localize in the first hydration layer. In verification calculations, when W4 was removed from the four solvation models, the proton of N1 was found to be always trapped by the O6 atom of $G^{\bullet+}$, eventually forming an intramolecular hydrogen transfer product rather than an expected deprotonation product (Figure S1), regardless of the solvation model used. This is the reason why the explicit water W4 in the second hydration shell is included in each model.

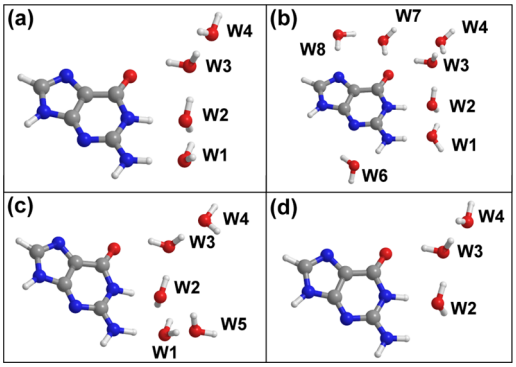

Figure 2. Arrangements of explicit waters in the (a) $4H_2O$-PCM, (b) $7H_2O$-PCM, (c) $5H_2O$-PCM, and (d) $3H_2O$-PCM models. Carbon, oxygen, nitrogen, and hydrogen atoms are denoted with gray, red, blue, and white balls, respectively.

Figure 3a displays the potential energy profile for deprotonation from N1 site calculated under the $4H_2O$-PCM model. Initially, the reactant $G^{\bullet+}$ and the four water molecules form a complex $G^{\bullet+}\cdots 4H_2O$ shown in Figure 2a. Accompanying the cleavage of N1−H^+ bond of the complex, the proton H^+ gradually moves to W2, leading to a transition state (TS) with an energy barrier of 13.4 kJ/mol. In the optimized TS structure, the proton does not localize at the W2 but forms a proton bridge between W2 and W3. Sequentially, the H^+ proceeds to transport along the proton bridge and, finally, is stabilized at W3. In the structure of the reaction product, the H^+ completely escapes from the N1−H site of G, indicating the generation of $G(N1-H)^{\bullet}$. This energy profile describes that $G^{\bullet+}$ deprotonates to $G(N1-H)^{\bullet}$ by releasing a proton from N1 to the first hydration shell.

To confirm this proton transfer process, partial atomic charges through the NBO scheme are studied (Table 1). In the initial complex of $G^{\bullet+}\cdots 4H_2O$, the positive charge is mainly localized on a guanine base (+0.892|e|), while the surrounding water molecules remain almost neutral. For the TS and

Table 1. Molecular Charge (|e|) Distribution for Each Optimized Structure in the $4H_2O$-PCM Model Calculated at the PCM/M06-2X/6-31++G level[a]**

	R	TS	P
G	0.892	0.177	0.176
W2···H···W3		0.729	
W3	0.020	0.119	0.693

[a]R: $G^{\bullet+}\cdots 4H_2O$. TS: $G(N1-H)^{\bullet}\cdots 2H_2O{\cdot}H^{+}{\cdot}2H_2O$,. P: $G(N1-H)^{\bullet}\cdots H_3O^{+}{\cdot}3H_2O$.

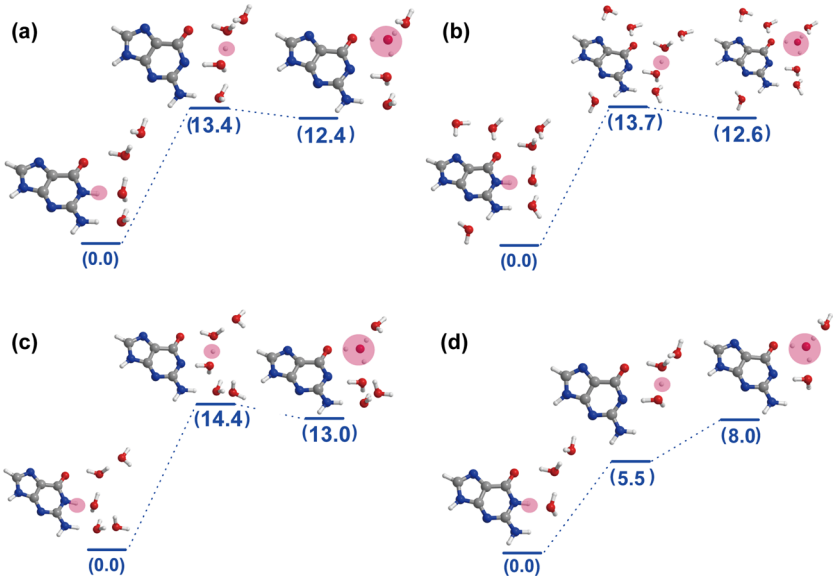

Figure 3. Potential energy profiles for the deprotonation of $G^{\bullet+}$ under (a) $4H_2O$-PCM, (b) $7H_2O$-PCM, (c) $5H_2O$-PCM, and (d) $3H_2O$-PCM models. The energies (in kJ/mol) are obtained at the PCM/M06-2X/6-31++G** level. Carbon, oxygen, nitrogen, and hydrogen atoms are denoted with gray, red, blue, and white balls, respectively. The pink circle highlights the migrated proton.

https://dx.doi.org/10.1021/acs.jpca.0c03748
J. Phys. Chem. A 2020, 124, 6076−6083

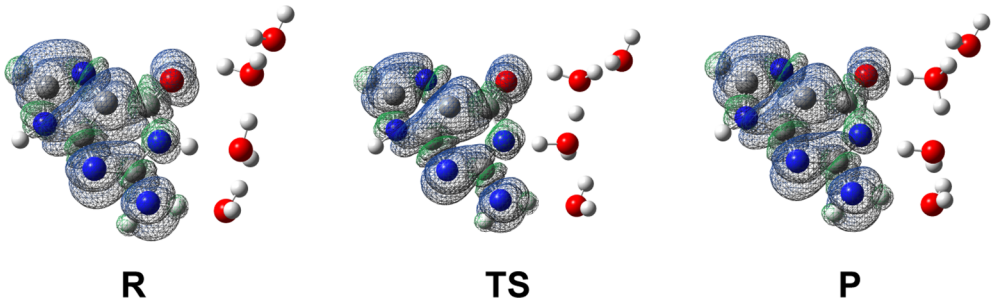

Figure 4. Spin density distribution for each optimized structure in the $4H_2O$-PCM model calculated at the PCM/M06-2X/6-31++G** level. Carbon, oxygen, nitrogen, and hydrogen atoms are denoted with gray, red, blue, and white balls, respectively. R: $G^{\bullet+}\cdots 4H_2O$. TS: $G(N1-H)^{\bullet}\cdots 2H_2O{\cdot}H^{+}{\cdot}2H_2O$. P: $G(N1-H)^{\bullet}\cdots H_3O^{+}{\cdot}3H_2O$.

deprotonation product, the positive charge mainly distributes in the surrounding waters (+0.848|e| for TS and 0.693|e| for deprotonation product), instead of the G base. From the values listed in Table 1, it is found that the proton is indeed transferred from G to the surrounding waters. Additional spin density calculations show that, for each optimized structure, the single unpaired electron is always restricted on the G base, as shown in Figure 4. This further demonstrates that the calculated process reflects the transport of the proton rather than a hydrogen atom.

It is noticeable that the product complex lies 12.4 kJ/mol above the reactant. To verify the energy predicted, empirical terms that model dispersion interactions were added to the M06-2X functional to consider long-range electron correlation. It is shown that the energy of product predicted by the M06-2X-D3 functional is still 12.6 kJ/mol above the reactant, thereby confirming the M06-2X result. In fact, proton release of $G^{\bullet+}$ described by Figure 3a only corresponds to the first step of deprotonation of $G^{\bullet+}$. Complete deprotonation of $G^{\bullet+}$ should also include the second step, the proton being transferred from the first hydration shell to the outer hydration shell. For the overall deprotonation process, the calculated product $G(N1-H)^{\bullet}\cdots H_3O^{+}{\cdot}3H_2O$ in Figure 3a is merely a key intermediate species. For the second step of deprotonation of $G^{\bullet+}$, i.e., proton mobility in bulk water, a widely accepted understanding is that its transport efficiency is abnormally high.[3] Nuclear magnetic resonance (NMR) and ^{17}O resonance,[53,54] Rayleigh light scattering,[55] and inelastic neutron scattering[56] experiments have suggested that proton hopping times are about 1−2 ps at room temperature. Therefore, for overall deprotonation process on the time scale of nanoseconds, the second step, the proton diffusing into outer hydration shell is not the rate-determining step. It follows that the migration of H^{+} to the first hydration shell should be a key step of the deprotonation process, i.e., the rate-determining step. Thus, the calculated reaction energy barrier of 13.4 kJ/mol can be approximately determined as its activation energy for the overall process, which is in good agreement with our experimental value.

To further validate the model, the influences of explicit water numbers on the energetics of deprotonation are examined. For the $4H_2O$-PCM model, all the explicit waters (W1, W2, W3, and W4) arrange near the deprotonation site. To avoid ignoring influence of waters far from the deprotonation site, three more waters are added near the remaining exterior atoms of $G^{\bullet+}$ on the basis of the initial $G^{\bullet+}\cdots 4H_2O$ structure, as shown in Figure 2b. The $7H_2O$-PCM model predicts the energy barrier of 13.7 kJ/mol, nearly the same as that of the $4H_2O$-PCM model (Figure 3b and Table S2). This demonstrates that the influence of the water molecules far from the deprotonation site is not significant for the deprotonation process of $G^{\bullet+}$. In order to explore whether more explicit waters are required in the second hydration layer, another water is added in the second hydration, and the $5H_2O$-PCM model is proposed (Figure 2c). It is shown that the $5H_2O$-PCM model also obtains a nearly identical energy barrier (14.4 kJ/mol) and the same deprotonation route (Figure 3c and Table S2), compared with results for the $4H_2O$-PCM model. This result indicates that adding more water molecules in the second hydration shell hardly alters the proton transport route and deprotonation energy barrier.

Furthermore, the effect of including fewer waters on deprotonation is also investigated. According to the $4H_2O$-PCM, $5H_2O$-PCM, and $7H_2O$-PCM results, it is inferred that W2 and W3 directly participate in deprotonation as a transfer and an acceptor, while W4 helps the proton to escape the trap of the O6 atom and to be stabilized in W3. Obviously, the three explicit waters (W2, W3, and W4) are required for any solvation model. As for W1, it does not directly take part in the proton transfer progress and seems dispensable. To determine its role in deprotonation, the $3H_2O$-PCM model is used by removing W1 (Figure 2d). As shown in Figure 3d and Table S2, a similar proton transfer occurs under the $3H_2O$-PCM model, but the energy barrier is merely 5.5 kJ/mol, lower than those of the other three models. Disappearance of a hydrogen bond formed by W1 with W2 should be the main reason for the reduced energy barrier, indicating that W1 has a strong influence on energetics of the deprotonation.

In comparison with the experimental activation energy, it is found that the $3H_2O$-PCM result deviates obviously, while results of the $4H_2O$-PCM, $5H_2O$-PCM, and $7H_2O$-PCM models all fall into the range of allowable error. It can be concluded that except for the $3H_2O$-PCM model, the results of the other three models are reasonable. This indicates that properly simulating the surrounding environment of $G^{\bullet+}$ requires at least four explicit waters. Adding more water molecules far away from the deprotonation site has little influence.

As shown in the potential energy profile of the $4H_2O$-PCM model (Figure 2a), in the product structure, four waters are hydrogen bonded with each other. According to NBO results, the migrated proton is mainly accepted by W2, thereby leading to a H_3O^{+} moiety bound with the O6 atom of $G(N1-H)^{\bullet}$ and two H_2O molecules (W2 and W4). Such a structure of protonated surrounding waters is similar to that of $H_9O_4^{+}$ in

https://dx.doi.org/10.1021/acs.jpca.0c03748
J. Phys. Chem. A 2020, 124, 6076−6083

water wires (Figure S2); thus, the product is actually a neutral G(N1−H)• in complex with a protonated water cluster of $H_9O_4^+$. Indeed, the NBO results show that $H_9O_4^+$ has already existed in the TS geometry, in which a proton is shared between W2 and W3 (∼1.2 Å from each oxygen atom) in a nearly linear O(W2)−H−O(W3) arrangement (∼170°). This structure is similar to that of another important protonated water cluster in water wires, $H^+(H_2O)_2$ with a proton bridge between two waters (Figure S2). This structural characteristic indicates that TS tends to transfer a proton to yield deprotonation product G(N1−H)•···$H_9O_4^+$, suggesting the protonated water cluster of $H_9O_4^+$ facilitates deprotonation of $G^{\bullet+}$. Compared with previous theoretical results in the presence of a single water,[29] the involvement of a protonated water cluster in the 4H_2O-PCM model significantly improves the theoretical prediction of the energy barrier, allowing a nice agreement between theory and experiment. The results also indicate the crucial role of a protonated water cluster in the deprotonation of $G^{\bullet+}$, which should be an interesting topic for future spectroscopic studies.

CONCLUSIONS

By combining the method of quantum chemistry and technique of time-resolved laser flash photolysis spectroscopy, we investigated the deprotonation mechanism of $G^{\bullet+}$ generated from one-electron oxidation of free G base. Experimentally, the dependence of formation kinetics of G(N1−H)• on temperatures was monitored with the transient absorption spectroscopy, and the activation energy of $G^{\bullet+}$ deprotonation (15.1 ± 1.5 kJ/mol) is determined. To theoretically simulate surrounding environment of $G^{\bullet+}$, four solvation models (3H_2O-PCM, 4H_2O-PCM, 5H_2O-PCM, and 7H_2O-PCM) were proposed, in which the explicit waters in the first/second hydration layers and PCM model are used to reflect solvation effects of short-range hydrogen-bonding interactions and outer hydration sphere, respectively. On the basis of the models, potential energy profiles of deprotonation from N1 of $G^{\bullet+}$ were calculated at the M06-2X/6-31++G** level, in which activation energy values are predicted to be 5.5, 13.4, 14.4, and 13.7 kJ/mol for the 3H_2O-PCM, 4H_2O-PCM, 5H_2O-PCM, and 7H_2O-PCM models, respectively. Comparing experimental and theoretical data, it can be concluded that except for the 3H_2O-PCM model, results of the other three models are reasonable, showing that at least four explicit waters are required for properly simulating the deprotonation of $G^{\bullet+}$ in aqueous media. In the 4H_2O-PCM model, participation of protonated water cluster of $H_9O_4^+$ facilitates deprotonation of $G^{\bullet+}$. These results provide mechanistic insights for understanding the deprotonation of $G^{\bullet+}$ in free base, demonstrating the important role of protonated water cluster in proton transfer of nucleobase systems. In addition, the theoretical strategy employed here can provide guidance for analogous proton transfer processes in aqueous solution.

ASSOCIATED CONTENT

Supporting Information

The Supporting Information is available free of charge at https://pubs.acs.org/doi/10.1021/acs.jpca.0c03748.

Potential energy profile for $G^{\bullet+}$ with 3 waters in the first hydration, molecular structures, relative energies for deprotonation using BP86, PBE, B3LYP, and M06-2X-D3 functionals, molecular charge (lel) distributions, and Cartesian coordinates for optimized structures along potential energy profiles of Figure 3 (PDF)

AUTHOR INFORMATION

Corresponding Authors

Jialong Jie − *College of Chemistry, Beijing Normal University, Beijing 100875, P. R. China*; Email: jialong@bnu.edu.cn

Di Song − *Beijing National Laboratory for Molecular Sciences, Institute of Chemistry, Chinese Academy of Sciences, Beijing 100190, P. R. China*; orcid.org/0000-0002-8652-0896; Email: songdi@iccas.ac.cn

Authors

Xianwang Zhang − *Beijing National Laboratory for Molecular Sciences, Institute of Chemistry, Chinese Academy of Sciences, Beijing 100190, P. R. China; University of Chinese Academy of Sciences, Beijing 100048, P. R. China*

Hongmei Su − *College of Chemistry, Beijing Normal University, Beijing 100875, P. R. China*; orcid.org/0000-0001-7384-6523

Complete contact information is available at: https://pubs.acs.org/10.1021/acs.jpca.0c03748

Notes

The authors declare no competing financial interest.

ACKNOWLEDGMENTS

This work was financially supported by the National Natural Science Foundation of China (Grant No. 21933005, No. 21773257, No. 21425313, and No. 21373233).

REFERENCES

(1) Eigen, M. Proton Transfer, Acid-Base Catalysis, and Enzymatic Hydrolysis. Part I: Elementary Processes. *Angew. Chem., Int. Ed. Engl.* **1964**, *3*, 1−19.

(2) Zundel, G. Hydration Structure and Intermolecular Interaction in Polyelectrolytes. *Angew. Chem., Int. Ed. Engl.* **1969**, *8*, 499−509.

(3) Agmon, N. The Grotthuss Mechanism. *Chem. Phys. Lett.* **1995**, *244*, 456−462.

(4) Marx, D.; Tuckerman, M. E.; Hutter, J.; Parrinello, M. The Nature of the Hydrated Excess Proton in Water. *Nature* **1999**, *397*, 601−604.

(5) Smondyrev, A. M.; Voth, G. A. Molecular Dynamics Simulation of Proton Transport Near the Surface of a Phospholipid Membrane. *Biophys. J.* **2002**, *82*, 1460−1468.

(6) Lapid, H.; Agmon, N.; Petersen, M. K.; Voth, G. A. A Bond-Order Analysis of the Mechanism for Hydrated Proton Mobility in Liquid Water. *J. Chem. Phys.* **2005**, *122*, 014506.

(7) Markovitch, O.; Chen, H.; Izvekov, S.; Paesani, F.; Voth, G. A.; Agmon, N. Special Pair Dance and Partner Selection: Elementary Steps in Proton Transport in Liquid Water. *J. Phys. Chem. B* **2008**, *112*, 9456−9466.

(8) *The Hydrogen Bond. Recent Developments in Theory and Experiments*; Schuster, P., Zundel, G., Sandorfy, C., Eds.; North-Holland Publishing Company: Amsterdam, New York, 1976.

(9) Asmis, K. R.; Pivonka, N. L.; Santambrogio, G.; Brümmer, M.; Kaposta, C.; Neumark, D. M.; Wöste, L. Gas-Phase Infrared Spectrum of the Protonated Water Dimer. *Science* **2003**, *299*, 1375−1377.

(10) Song, D.; Su, H.; Kong, F.-a.; Lin, S.-H. Anharmonic RRKM Calculation for the Dissociation of $(H_2O)_2H^+$ and Its Deuterated Species $(D_2O)_2D^+$. *J. Phys. Chem. A* **2010**, *114*, 10217−10224.

(11) Garczarek, F.; Gerwert, K. Functional Waters in Intraprotein Proton Transfer Monitored by FTIR Difference Spectroscopy. *Nature* **2006**, *439*, 109−112.

(12) Candeias, L. P.; Steenken, S. Structure and Acid-Base Properties of One-Electron-Oxidized Deoxyguanosine, Guanosine, and 1-Methylguanosine. *J. Am. Chem. Soc.* **1989**, *111*, 1094−1099.
(13) Steenken, S. Purine Bases, Nucleosides, and Nucleotides: Aqueous Solution Redox Chemistry and Transformation Reactions of Their Radical Cations and e^- and OH Adducts. *Chem. Rev.* **1989**, *89*, 503−520.
(14) Steenken, S.; Jovanovic, S. V. How easily oxidizable is DNA? One-Electron Reduction Potentials of Adenosine and Guanosine Radicals in Aqueous Solution. *J. Am. Chem. Soc.* **1997**, *119*, 617−618.
(15) Giese, B.; Amaudrut, J.; Köhler, A.-K.; Spormann, M.; Wessely, S. Direct Observation of Hole Transfer through DNA by Hopping between Adenine Bases and by Tunnelling. *Nature* **2001**, *412*, 318−320.
(16) Li, X.; Cai, Z.; Sevilla, M. D. Investigation of Proton Transfer within DNA Base Pair Anion and Cation Radicals by Density Functional Theory (DFT). *J. Phys. Chem. B* **2001**, *105*, 10115−10123.
(17) Kobayashi, K.; Tagawa, S. Direct Observation of Guanine Radical Cation Deprotonation in Duplex DNA Using Pulse Radiolysis. *J. Am. Chem. Soc.* **2003**, *125*, 10213−10218.
(18) Adhikary, A.; Kumar, A.; Becker, D.; Sevilla, M. D. The Guanine Cation Radical: Investigation of Deprotonation States by ESR and DFT. *J. Phys. Chem. B* **2006**, *110*, 24171−24180.
(19) Ghosh, A. K.; Schuster, G. B. Role of the Guanine N1 Imino Proton in the Migration and Reaction of Radical Cations in DNA Oligomers. *J. Am. Chem. Soc.* **2006**, *128*, 4172−4173.
(20) Adhikary, A.; Kumar, A.; Khanduri, D.; Sevilla, M. D. Effect of Base Stacking on the Acid-Base Properties of the Adenine Cation Radical $[A^{\bullet+}]$ in Solution: ESR and DFT Studies. *J. Am. Chem. Soc.* **2008**, *130*, 10282−10292.
(21) Kobayashi, K.; Yamagami, R.; Tagawa, S. Effect of Base Sequence and Deprotonation of Guanine Cation Radical in DNA. *J. Phys. Chem. B* **2008**, *112*, 10752−10757.
(22) Kumar, A.; Sevilla, M. D. Influence of Hydration on Proton Transfer in the Guanine-Cytosine Radical Cation ($G^{\bullet+}$-C) Base Pair: A Density Functional Theory Study. *J. Phys. Chem. B* **2009**, *113*, 11359−11361.
(23) Wu, L.; Liu, K.; Jie, J.; Song, D.; Su, H. Direct Observation of Guanine Radical Cation Deprotonation in G-Quadruplex DNA. *J. Am. Chem. Soc.* **2015**, *137*, 259−266.
(24) Jie, J.; Liu, K.; Wu, L.; Zhao, H.; Song, D.; Su, H. Capturing the Radical Ion-Pair Intermediate in DNA Guanine Oxidation. *Sci. Adv.* **2017**, *3*, No. e1700171.
(25) Nir, E.; Kleinermanns, K.; de Vries, M. S. Pairing of Isolated Nucleic-Acid Bases in the Absence of the DNA Backbone. *Nature* **2000**, *408*, 949−951.
(26) Cerón-Carrasco, J. P.; Requena, A.; Perpète, E. A.; Michaux, C.; Jacquemin, D. Theoretical Study of the Tautomerism in the One-Electron Oxidized Guanine-Cytosine Base Pair. *J. Phys. Chem. B* **2010**, *114*, 13439−13445.
(27) Adhikary, A.; Khanduri, D.; Sevilla, M. D. Direct Observation of the Hole Protonation State and Hole Localization Site in DNA-Oligomers. *J. Am. Chem. Soc.* **2009**, *131*, 8614−8619.
(28) Candeias, L.; Steenken, S. Ionization of Purine Nucleosides and Nucleotides and Their Components by 193-nm Laser Photolysis in Aqueous Solution: Model Studies for Oxidative Damage of DNA. *J. Am. Chem. Soc.* **1992**, *114*, 699−704.
(29) Liu, N.; Ban, F.; Boyd, R. J. Modeling Competitive Reaction Mechanisms of Peroxynitrite Oxidation of Guanine. *J. Phys. Chem. A* **2006**, *110*, 9908−9914.
(30) Xia, Y.; Wang, F.; Wang, R.; Liu, K.; Su, H. Reaction Kinetics between Thiobases and Singlet Oxygen Studied by Direct Detection of the $^1O_2$ Luminescence Decay. *Chin. J. Chem. Phys.* **2019**, *32*, 93−98.
(31) Jie, J.; Wang, C.; Zhao, H.; Song, D.; Su, H. Experimental and Theoretical Study of Deprotonation of DNA Adenine Cation Radical. *Chin. J. Chem. Phys.* **2017**, *30*, 664−670.
(32) Zhao, Y.; Truhlar, D. G. How Well Can New-Generation Density Functionals Describe the Energetics of Bond-Dissociation Reactions Producing Radicals? *J. Phys. Chem. A* **2008**, *112*, 1095−1099.
(33) Zhao, Y.; Truhlar, D. G. The M06 Suite of Density Functionals for Main Group Thermochemistry, Thermochemical Kinetics, Noncovalent Interactions, Excited States, and Transition Elements: Two New Functionals and Systematic Testing of Four M06-Class Functionals and 12 Other Functionals. *Theor. Chem. Acc.* **2008**, *120*, 215−241.
(34) Valero, R.; Gomes, J. R. B.; Truhlar, D. G.; Illas, F. Good Performance of the M06 Family of Hybrid Meta Generalized Gradient Approximation Density Functionals on a Difficult Case: CO Adsorption on MgO(001). *J. Chem. Phys.* **2008**, *129*, 124710.
(35) Hohenstein, E. G.; Chill, S. T.; Sherrill, C. D. Assessment of the Performance of the M05-2X and M06-2X Exchange-Correlation Functionals for Noncovalent Interactions in Biomolecules. *J. Chem. Theory Comput.* **2008**, *4*, 1996−2000.
(36) Kumar, A.; Sevilla, M. D. Density Functional Theory Studies of the Extent of Hole Delocalization in One-Electron Oxidized Adenine and Guanine Base Stacks. *J. Phys. Chem. B* **2011**, *115*, 4990−5000.
(37) DeBlase, A. F.; Wolke, C. T.; Weddle, G. H.; Archer, K. A.; Jordan, K. D.; Kelly, J. T.; Tschumper, G. S.; Hammer, N. I.; Johnson, M. A. Water Network-Mediated, Electron-Induced Proton Transfer in $[C_5H_5N\bullet(H_2O)_n]^-$ Clusters. *J. Chem. Phys.* **2015**, *143*, 144305.
(38) Frisch, M. J.; Trucks, G. W.; Schlegel, H. B.; Scuseria, G. E.; Robb, M. A.; Cheeseman, J. R.; Scalmani, G.; Barone, V.; Mennucci, B.; Petersson, G. A.; et al. *Gaussian 09*, Revision E.01; Gaussian, Inc.: Wallingford, CT, 2013.
(39) Rokhlenko, Y.; Geacintov, N. E.; Shafirovich, V. Lifetimes and Reaction Pathways of Guanine Radical Cations and Neutral Guanine Radicals in an Oligonucleotide in Aqueous Solutions. *J. Am. Chem. Soc.* **2012**, *134*, 4955−4962.
(40) McElroy, W. J. A Laser Photolysis Study of the Reaction of Sulfate(1-) with Chloride and the Subsequent Decay of Chlorine(1-) in Aqueous Solution. *J. Phys. Chem.* **1990**, *94*, 2435−2441.
(41) Wang, Y.; Zhao, H.; Yang, C.; Jie, J.; Dai, X.; Zhou, Q.; Liu, K.; Song, D.; Su, H. Degradation of Cytosine Radical Cations in 2′-Deoxycytidine and in i-Motif DNA: Hydrogen-Bonding Guided Pathways. *J. Am. Chem. Soc.* **2019**, *141*, 1970−1979.
(42) Banyasz, A.; Martínez-Fernández, L.; Balty, C.; Perron, M.; Douki, T.; Improta, R.; Markovitsi, D. Absorption of Low-Energy UV Radiation by Human Telomere G-Quadruplexes Generates Long-Lived Guanine Radical Cations. *J. Am. Chem. Soc.* **2017**, *139*, 10561−10568.
(43) Banyasz, A.; Balanikas, E.; Martínez-Fernández, L.; Baldacchino, G.; Douki, T.; Improta, R.; Markovitsi, D. Radicals Generated in Tetramolecular Guanine Quadruplexes by Photoionization: Spectral and Dynamical Features. *J. Phys. Chem. B* **2019**, *123*, 4950−4957.
(44) Martínez Fernández, L.; Cerezo, J.; Asha, H.; Santoro, F.; Coriani, S.; Improta, R. The Absorption Spectrum of Guanine Based Radical: A Comparative Computational Analysis. *ChemPhotoChem.* **2019**, *3*, 846−855.
(45) Naumov, S.; von Sonntag, C. Guanine-Derived Radicals: Dielectric Constant-Dependent Stability and UV/Vis Spectral Properties: a DFT Study. *Radiat. Res.* **2008**, *169*, 364−372.
(46) Rickert, K. W.; Klinman, J. P. Nature of Hydrogen Transfer in Soybean Lipoxygenase 1: Separation of Primary and Secondary Isotope Effects. *Biochemistry* **1999**, *38*, 12218−12228.
(47) Knapp, M. J.; Rickert, K.; Klinman, J. P. Temperature-Dependent Isotope Effects in Soybean Lipoxygenase-1: Correlating Hydrogen Tunneling with Protein Dynamics. *J. Am. Chem. Soc.* **2002**, *124*, 3865−3874.
(48) Hatcher, E.; Soudackov, A. V.; Hammes-Schiffer, S. Proton-Coupled Electron Transfer in Soybean Lipoxygenase: Dynamical Behavior and Temperature Dependence of Kinetic Isotope Effects. *J. Am. Chem. Soc.* **2007**, *129*, 187−196.
(49) Tautermann, C. S.; Loferer, M. J.; Voegele, A. F.; Liedl, K. R. Double Hydrogen Tunneling Revisited: The Breakdown of

https://dx.doi.org/10.1021/acs.jpca.0c03748
J. Phys. Chem. A 2020, 124, 6076−6083

Experimental Tunneling Criteria. *J. Chem. Phys.* **2004**, *120*, 11650−11657.
(50) Stojković, V.; Kohen, A. Enzymatic H Transfers: Quantum Tunneling and Coupled Motion from Kinetic Isotope Effect Studies. *Isr. J. Chem.* **2009**, *49*, 163−173.
(51) Knapp, M. J.; Klinman, J. P. Environmentally Coupled Hydrogen Tunneling. *Eur. J. Biochem.* **2002**, *269*, 3113−3121.
(52) Jonsson, T.; Glickman, M. H.; Sun, S.; Klinman, J. P. Experimental Evidence for Extensive Tunneling of Hydrogen in the Lipoxygenase Reaction: Implications for Enzyme Catalysis. *J. Am. Chem. Soc.* **1996**, *118*, 10319−10320.
(53) Meiboom, S. Nuclear Magnetic Resonance Study of the Proton Transfer in Water. *J. Chem. Phys.* **1961**, *34*, 375−388.
(54) Montrose, C. J.; Bucaro, J. A.; Marshall-Coakley, J.; Litovitz, T. A. Depolarized Rayleigh Scattering and Hydrogen Bonding in Liquid Water. *J. Chem. Phys.* **1974**, *60*, 5025−5029.
(55) Conde, O.; Teixeira, J. Hydrogen Bond Dynamics in Water Studied by Depolarized Rayleigh Scattering. *J. Phys. (Paris)* **1983**, *44*, 525−529.
(56) Bellissent-Funel, M.-C.; Teixeira, J. Dynamics of Water Studied by Coherent and Incoherent Inelastic Neutron Scattering. *J. Mol. Struct.* **1991**, *250*, 213−230.

https://dx.doi.org/10.1021/acs.jpca.0c03748
J. Phys. Chem. A 2020, 124, 6076−6083